Report on Experiment # HS-1604

Introduction

The redox conditions and oxygen fugacity (fO_2) in the lowermost mantle remain uncertain. The Al-bearing $(Mg,Fe)SiO_3$ bridgmanite (Bg) strongly favours the couple substitution of Fe^{3+} and Al^{3+} cations in the $A^{2+}B^{4+}O_3$-based perovskite-type lattice. The Al-Fe^{3+} interaction in this phase is such that it induces the Fe^{2+} disproportionation into Fe^{3+} and Fe^0 [1]. This property dominates the redox state of the shallow lower mantle. However, there are major parameters that can affect the redox properties deeper in the mantle: (i) A progressive spin transition in Fe was reported for Bg between 70 and 120 GPa [2]. (ii) Phase transformation from Bg to post-Bg (PBg) occurs above 120 GPa [3]. The PBg structure is analogue to $CaIrO_3$, with some SiO_6 octahedral sharing edges instead of corners in the perovskite, which could modify drastically the PBg crystal chemistry, compared to Bg (see [4]). (iii) The presence of (Mg,Fe)O ferropericlase (Fp), the second major mineral in the lower mantle, could affect significantly the behavior of Fe; In particular, Fe undergoes a spin transition in Fp at lower mantle pressures (e.g. [5]). Finally, the mantle may undergo partial melting in the D"-layer [6]. All these transitions can modify drastically the Al, Fe^{2+} and Fe^{3+} chemical activities and therefore the redox properties.

In order to improve our knowledge on the crystal chemistry of Bg and PBg and the redox state in the lower mantle, we performed X-ray Absorption Spectroscopy (XAFS) at the Fe K-edge *in situ* in the diamond anvil cell (DAC) at pressures up to 130 GPa, using the ID24 beamline at ESRF.

Methods

We prepared two powder mixture as starting materials: $(Mg,Fe)_2SiO_4$-olivine plus Al_2O_3 and Al-bearing $(Mg,Fe)SiO_3$-enstatite plus Fp. Also, we used starting material made of the pure end-member components, Al-bearing $(Mg,Fe)SiO_3$-enstatite and Fp. Both sample mixtures are expected to yield the same mixture of Al-bearing $(Mg,Fe)SiO_3$ Bg plus Fp at lower mantle P and T conditions. The use of the two different mixtures can help to insure reproducibility of our results. In order to prevent water contamination, powders were finely grinded in a glove bag with an argon flow just before the loading in the pressure chamber.

We used membrane type DAC mounted with diamonds with beveled culets with diameters from 250/300 to 75/300 µm, depending on the target pressure. We selected diamond anvils of 1.6 mm height in order to reduce their absorption of X-rays at the Fe K-edge energy (7112 eV). The samples were loaded in gasket holes bigger than 40 µm, together with a piece of KCl that was used as a reference for the X-ray beam intensity (I_0).

After the target pressure was achieved, we performed the phase transition typical of lower mantle mineralogy using two fiber lasers of 100 W each, with the on-line system available at ID24 (Ref. Kantor). The lasers were focused to ~25 µm hot spot on the sample, using lenses of 50 mm focal length. The temperatures was monitored by thermal radiometry and progressively increased up to more than 2500 K. At each temperature investigated, we scanned slowly the sample between the two lasers to anneal the whole sample volume, for about 30 minutes, before the lasers were quenched. We used one fresh sample per pressure condition. This procedure prevents potential problems associated to slow atomic diffusion between the grains, which average size had increased after the consecutive laser annealing at a given pressure.

Pressures at 300 K were derived from the shift of the major Raman peak of diamond surface in contact with the sample. However, samples submitted to laser heating encounter an increase of pressure due to the effect of thermal pressure [7]. We can estimate the pressure at high-T from the nominal pressure by applying a pressure correction of $0.5\ 10^{-3}$ GPa/K, which corresponds to ~50% of the theoretical thermal pressure ($\alpha K \Delta T$) of the main mineral present in our samples, Bg or PBg. Final error in pressure is estimated to be 5%.

The XAFS measurements were performed at the Fe K-edge using dispersive µ-XANES spectroscopy at the ID24 beamline [8]. We used the Si(220) bent crystal polychromator that provides the best compromise between spectral resolution for pre-edge absorption peak analysis, X-ray flux,

and k-space extension. The polychromatic X-ray beam was focused to a ~5×5 µm spot onto the sample. The absorption spectrum µ(E) is equal to $\ln(I_0/I_1)$ where I_0, and I_1, are the X-ray intensities recorded by the spatially resolved CCD detector at the sample position, and in a piece of KCl, respectively. Both I_0 and I_1 were measured through the diamonds to improve the quality of the absorption signal. The diamond anvil cell was rotated in the X-ray beam to remove the diffraction peaks of diamonds from the energy range of interest. Using the dispersive mode, acquisition time is reduced to a few minutes. To improve statistics and prevent from potential artefacts related to grain growth and sample heterogeneity, we performed sample maps with a spatial resolution of ~5x5 µm. Recorded XAFS signals on these maps were then averaged [9].

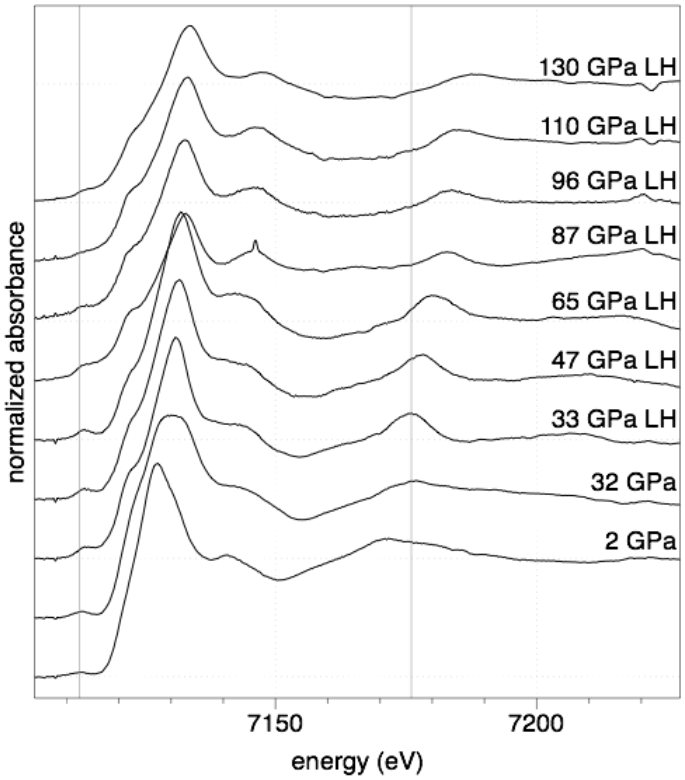

Fig. 1: Evolution with pressure of the Fe absorption K-edge in the sample made of olivine plus corundum. "LH" indicates spectra recorded after laser annealing. The first vertical shaded line shows the position of pre-edge region (see zoom in Fig. 2). The second is the first maximum of EXAFS oscillations, which clearly shifts toward higher energy with increasing pressure.

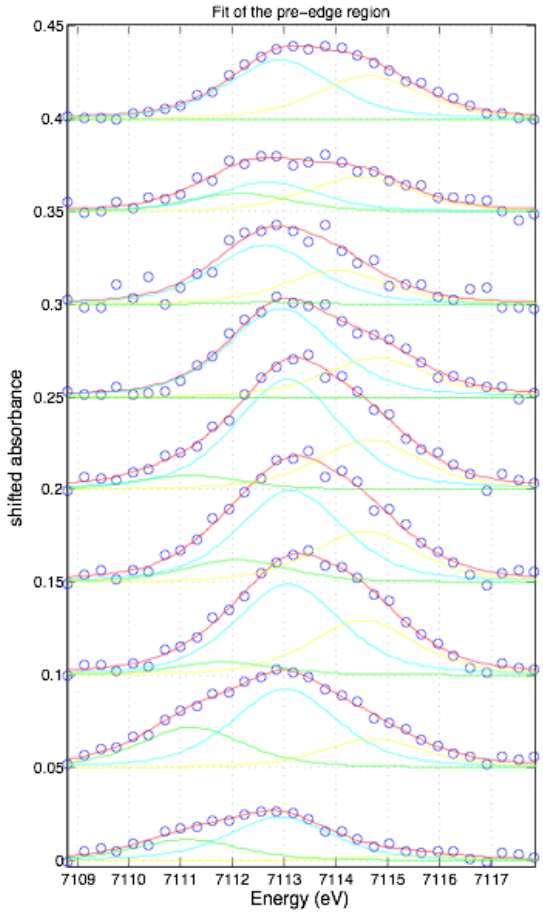

Fig. 2: Zoom of the pre-edge region of the XAFS patterns. To refine the sample redox state, we performed fits (blue and green fine lines) of pre-peaks using 2 or 3 Gaussian contributions.

Preliminary results

We report the normalized X-ray absorption signal of the mixture of olivine plus corundum as a function of pressure (Fig. 1). The pattern changes significantly before (32 GPa) and after laser heating (33 GPa LH) due to olivine decomposition into Bg and Fp and chemical reaction with corundum. At each pressure above 32 GPa, no significant change was observed when we performed additional laser heating at higher temperature or for longer duration. The pressure sequence shows a clear shift toward higher energies, from ~7175 to 7190 eV, of the first maximum of the EXAFS oscillations. This can be related to the compression of the first shell of oxygen atoms around Fe, making the Fe-O EXAFS oscillation wider.

In addition, the shape of XANES changes significantly between 65 and 87 GPa. It is the pressure range where Fe undergoes a high-spin to low-spin transition in the Fp phase [5], a transition is associated with reduction of the Fe volume. At similar pressures, the Fe spin transition in Bg was reported to be possibly initiated, but certainly it remains incomplete up to much higher pressures [2,10,11]. The difference in Fe behavior between the two phases is likely to include a major change in the Fe-behavior, which can explain the experimental features; Al-bearing Bg is an important host for Fe at lower pressures [12] and more Fe is included in Fp at higher pressures after the change of spin of Fe. We do not observe any discontinuous change after 87 GPa up to the maximum nominal pressure of 130 GPa performed in this study. To enable a quantitative decomposition of the XANES signals in a sum of Bg (or PBg) and Fp, as performed in our previous study [4], we measured the XANES signature of the two end-members materials, Bg and Fp, by two independent compression up to more than 100 GPa. The signal decomposition is in progress.

The pre-edge region of the absorption pattern can also constrain the sample state (Fig. 2). Like XANES features, we observe a clear change between 65 and 87 GPa, with appearance of a doublet peak, instead of a broad singlet at lower pressures. This change is correlated with a decrease of the intensity of the pre-peak contribution found at lower energy (7112-7113 eV) that is not visible in Fig. 2, due to normalization of the signal amplitude. These changes can also be related to the change in Fe-partitioning between Bg and Fp. We performed sum decomposition of the pre-edge in order to tentatively extract information on the $Fe^{3+}/(Fe^{3+}+Fe^{2+})$ ratio in the sample [13], using a similar technique than in our previous work [14]. The calculations are in progress.

Conclusions

Our results suggest a change in Fe partitioning coefficient between Bg and Fp in the 65 and 87 GPa pressure range. It is compatible with previous reports of a rapid change of Fe spin state in Fp. After further pressure increase to a nominal pressure of 130 GPa (corresponding to ~140 GPa at the annealing temperature of 2500 K), we do not observe any major change of the XAFS signal. It suggests that the occurrence of PBg phase, if it was indeed synthesized in this study, should not modify significantly the redox state of the lowermost mantle compared to Bg. Therefore, the lowermost mantle is likely to present the following mixture of Fe-bearing phases: a Fp enriched in FeO together an Al-bearing Bg and/or PBg phases relatively depleted in Fe, but with a relatively high $Fe^{3+}/(Fe^{3+}+Fe^{2+})$ ratio [14]. A high FeO-content in Fp suggest a relatively high fO_2 at the core mantle boundary. This should not favor the rejection to the lowermost mantle of oxygen atoms released to the outer core by inner core crystallization [15].

References:

1 Lauterbach, S. et al. *Contribution in Mineralogy and Petrology* **138**, 17, (2000).
2 Badro, J. et al. *Science* **305**, 383, (2004).
3 Murakami, M. et al. *Science* **304**, 855, (2004).
4 Andrault, D. et al. *Earth Planet. Sci. Lett.* **293**, 90, (2010).
5 Badro, J. et al. *Science* **300**, 789, (2003).
6 Lay, T. et al. *Physics of the Earth and Planetary Interior* **146**, 441, (2004).
7 Andrault, D. et al. *European Journal of Mineralogy* **10**, 931, (1998).
8 Pascarelli, S. et al. *J. Synchr. Rad.* **13**, 351, (2006).
9 Muñoz, M. et al. *Geochem., Geophys., Geosyst.* **7**, Q11020, (2006).
10 Li, L. et al. *Geophys. Res. Lett.* **32**, L17307, (2005).
11 Lin, J. F. et al. *Science* **317**, 1740, (2007).
12 Wood, B. J. & Rubie, D. C. *Science* **273**, 1522, (1996).
13 Wilke, M. et al. *Am. Miner.* **86**, 714, (2001).
14 Bolfan-Casanova, N. et al. *Am. Miner.* **97**, 1483, (2012).
15 Alfè, D. et al. *Mineralogical Magazine* **67**, 113, (2003).